Hybrid Magnetoelectric Nanowires for Nanorobotic Applications: Fabrication, Magnetoelectric Coupling, and Magnetically Assisted In Vitro Targeted Drug Delivery

Journal Article

Author(s):
Chen, Xiang-Zhong; Hoop, Marcus; Shamsudhin, Naveen; Huang, Tianyun; Özkale, Berna; Li, Qian; Siringil, Erdem; Mushtaq, Fajer; Di Tizio, Luca; Nelson, Bradley J.; Pané, Salvador

Publication date:
2017-02-24

Permanent link:
https://doi.org/10.3929/ethz-b-000124903

Originally published in:
Advanced Materials 29(8), https://doi.org/10.1002/adma.201605458

Funding acknowledgement:
336456 - Magnetoelectric chemonanorobotics for chemical and biomedical applications (EC)

Hybrid Magnetoelectric Nanowires for Nanorobotic Applications: Fabrication, Magnetoelectric Coupling and Magnetically-assisted *in vitro* Targeted Drug Delivery

*By Xiang-Zhong Chen, Marcus Hoop, Naveen Shamsudhin, Tianyun Huang[†], Berna Özkale, Qian Li, Erdem Siringil, Fajer Mushtaq, Luca Di Tizio, Bradley J. Nelson, and Salvador Pané**

[*] Dr. X. Z. Chen, M. Hoop, N. Shamsudhin, Dr. T. Huang, Dr. B. Özkale, E. Siringil, F. Mushtaq, L. Di Tizio, Prof. Dr. B. J. Nelson, Dr. S. Pané

Multi-Scale Robotics Lab (MSRL), Institute of Robotics & Intelligent Systems (IRIS), ETH Zurich, Zurich 8092, Switzerland

Dr. Q. Li

Center for Nanophase Materials Sciences and Institute for Functional Imaging of Materials, Oak Ridge National Laboratory, Oak Ridge, Tennessee 37831, USA

[†] Present Address: State Key Laboratory for Turbulence and Complex Systems, Beijing Innovation Center for Engineering Science and Advanced Technology (BIC-ESAT), College of Engineering, Peking University, Beijing, 100871, People's Republic of China

E-mail: vidalp@ethz.ch

Keywords: Nanorobotics, Magnetoelectric, P(VDF-TrFE), FeGa, Ferroelectric

Micro- and nanorobots are promising candidates for targeted therapeutic interventions and controlled drug delivery.[1] The primary advantage of these micro- and nanodevices over other small-scale therapeutic delivery systems is their controlled locomotion and thus accurate targeting ability.[2] Examples of such robots include surface-functionalized magnetic helical microswimmers and stimuli-responsive robots, which are able to target single cells and tissue locations for drug, gene or cell delivery.[1b, 3] The cargo release process in these small robots is usually triggered passively by localized changes in physiological conditions (e.g. pH, temperature) at the target site. However, possible off-target therapy delivery can be caused by complicated physiological conditions or unexpected changes of the local environment. Therefore, developing an integrated mobile micro- or nanorobot, which can be externally triggered will provide an alternative delivery strategy that is more controllable and favorable. Ideally, a therapeutic delivery platform should utilize the same external power source independently both for locomotion and for on-demand triggered therapeutics. However, to avoid interference between these two tasks is challenging using the same energy source.

In this work, we designed and fabricated wire-shaped magnetoelectric nanorobots to demonstrate a proof-of-concept integrated device, which is featured by wireless locomotion and on-site triggered therapeutic release using a single external power source (i.e. magnetic field). Among various techniques available to date for the wireless actuation of micro- and nanorobots,[2a, 2b, 4] the use of magnetic fields has been widely adopted due to their versatility and precision in controlling the locomotion of magnetic structures, and their excellent biocompatibility.[5] Magnetoelectric materials change their electric polarization when subject to appropriate magnetic stimulation, and it has been previously demonstrated that changes in the electric polarization can induce redistribution of surface charges, which is able to trigger chemical and/or biochemical

processes.[6] Here, we show that the integration of magnetoelectric materials in nanororobotic platforms not only enables the device to be precisely steered towards a targeted location by means of wireless magnetic fields, but also allows the device to perform on-demand magnetoelectrically-assisted drug release to cells.

We have designed a hybrid magnetoelectric core-shell composite nanowire with a magnetostrictive core and a piezoelectric shell. Poly(vinylidene fluoride-trifluoroethylene) P(VDF-TrFE), a piezoelectric polymer, is first fabricated into nanotube arrays through a template-based wetting technique.[7] In the second step, FeGa, an alloy with a large magnetostrictive coefficient, is electrodeposited inside the tubes to form the core-shell nanowire (**Figure 1**). Energy dispersive X-ray (EDX) analysis indicates a compositional ratio of $Fe_{80}Ga_{20}$ (Figure S1), which is reported to have the highest magnetostrictive coefficient (~400 ppm).[8] Upon magnetic stimulation, the magnetostrictive FeGa core deforms, and the strain is transferred onto the piezoelectric P(VDF-TrFE) shell, inducing changes in its surface polarization. Compared with single-phase magnetoelectric materials, this biphasic core-shell configuration provides more flexibility in design and fabrication of the device, ranging from material selection to morphology control of individual phases (e.g. thickness, length, etc.). Finally, FeGa@P(VDF-TrFE) core-shell nanowires are released by dissolving the template in NaOH solution and the gold plug layer in gold etchant.

The surface morphology of the hybrid nanowires is investigated by atomic force microscopy (AFM) in semi-contact mode (Figure 1b). Two distinct regions are clearly observed on each nanowire, as indicated by the dashed lines. While the upper parts reveal the smooth surface of FeGa grown out of the P(VDF-TrFE) nanotubes, the lower regions show random striped patterns, indicating the crystalline lamella of the polymer. Transmission electron microscopy (TEM)

(Figure 1c) reveals the conformal growth of FeGa nanowire inside the polymer tube, which replicates its inner rough surface. The FeGa core has a diameter of ~250 nm and the P(VDF-TrFE) shell has a thickness of ~35 nm (Figure 1c inset shows a cross-sectional thickness profile), which corresponds well to the pore diameter of the AAO template (300~350 nm). The rough stripe patterns of the outer shell are indications of crystal lamellar structures of P(VDF-TrFE). The crystalline nature is a prerequisite for nanoscale ferroelectricity in P(VDF-TrFE) [9]. The conformal growth of FeGa core and the absence of voids between the core and P(VDF-TrFE) shell ensures a solid interface junction, which is crucial for effective strain transfer from the magnetostrictive phase to the piezoelectric phase, thus, ensuring a large magnetoelectric effect.[10]

The infrared (IR) spectrum and X-Ray diffraction (XRD) patterns reveal the crystalline structure of the two phases. The IR spectrum (Figure 1d) shows characteristic absorption bands of ferroelectric crystalline phase in P(VDF-TrFE) (i.e., 1287 and 846 cm^{-1}, assigned to the ~~zigzag~~ chain conformations with three or more trans-isomer unit sequences, denoted as $T_{m\geq3}$).[11] The XRD pattern further corroborates the existence of ferroelectric crystals (Figure 1e), as evidenced by the diffraction peak at 20.3° which reflects the (110, 200) crystallographic plane with an interchain lattice space of 4.37 Å in ferroelectric β phase.[9b, 11b] The diffraction peaks located at 44.7°, 64.0° and 81.7°, corresponding to lattice constants of 2.03 Å, 1.45 Å and 1.18 Å, represent the (110), (211) and (200) crystallographic planes of FeGa, respectively. The lattice constants are slightly larger than that of disordered body-centered-cubic α-Fe (JCPDS 06-0696), which has lattice constants of 2.02 Å 1.43 Å 1.17 Å for (110), (211) and (200) crystalline plane. The incorporation of Ga atoms expands the lattice.[12] Selected area electron diffraction (SAED) pattern of a single nanowire also shows similar results. The multiple smeared diffraction rings corresponding to the same phase as determined from XRD are observed, indicating its

polycrystalline nature. However, some bright spots are also observed on the (110) ring, which proves that the FeGa nanowire has a preferred orientation along the <110> direction.

The ferroelectricity and magnetoelectricity of the core-shell nanowire can be directly probed using piezoresponse force microscopy (PFM) under an external magnetic field. An alternating voltage is applied to the sample using a conductive cantilever tip in contact mode to induce piezoelectric surface oscillations in the sample, which is sensed through the resulting cantilever deflection. **Figure 2** shows the PFM phase (a, c) and amplitude (b, d) images before and after applying an external magnetic field. The PFM phase image (Figure 2a) shows clear phase contrast between different regions, indicating anti-parallel domains with opposite out-of-plane polarization orientation, although the spatial distribution of the domains on the polymer shell is random. The amplitude image (Figure 2b) also shows distinct and randomly distributed piezoresponse on the shell. The random distribution of ferroelectric domains corresponds to the polycrystalline nature of the polymer. Upon application of an external magnetic field (1000 Oe, which is much larger than the coercive field of FeGa, Figure S2), no morphology change is observed (Figure S3). However, changes in ferroelectric domains are clearly observed in the PFM phase image and amplitude image. As can be seen from phase images (Figure 2a, c), while some of the bright regions grow at the expense of the dark regions (denoted by horizontal blue arrows), some of the dark areas turn bright (denoted by vertical yellow arrows). These changes are indicative of polarization reversal induced by magnetic field in certain ferroelectric domains. The effect of the magnetic field on the piezoresponse amplitude is clearly visible. While some domains with low initial amplitudes exhibit high amplitudes upon application of a magnetic field (denoted by the dashed square), others with high amplitudes show the opposite trend (denoted by the dashed circle). When an external magnetic field is applied, the magnetostrictive FeGa is strained. The

strain is then transferred to the piezoelectric P(VDF-TrFE) shell through interfacial coupling, which induce changes in the polarization state of P(VDF-TrFE). The polarization reversal and changes in piezoresponse caused by magnetic field induced strain are direct evidence of strong magnetoelectric coupling between the ferromagnetic and ferroelectric materials.[13]

To further investigate the ferroelectricity and the magnetoelectric coupling effect in the core-shell nanowire, local piezoresponse hysteresis loops are acquired at random locations on the wire (Figure 2e and f). The programmed excitation voltage waveform is a stepwise increasing, pulsed DC field superimposed with a small AC voltage. To minimize the possible interference of electrostatic forces, the AC piezoresponse signal was acquired during the off-phase of the bias pulse sequence.[14] The P(VDF-TrFE) shell exhibits polarization reversibility both with and without the application of a magnetic field, i.e., the polarization directions can be switched at both polarities of tip DC-bias voltages. The average phase contrast is close to 180°, confirming that the response is contributed by electromechanical response instead of electrostatic force.[15] Both piezoresponse phase loops are horizontally shifted, as also observed from the amplitude curves with asymmetric butterfly shape. The asymmetry of the loops can originate from different reasons, such as the imprint effect, internal bias fields inside the materials, and/or a work function difference between the top electrode (Pt-coated silicon probe) and the bottom electrode (FeGa).[9a, 9b, 13b, 16] The coercive voltages for the shell measured without magnetic field are −5.18 V and 1.56 V, respectively. Assuming that the electric field generated by the probe tip is uniform, and a 35 nm thickness of the P(VDF–TrFE) shell, the apparent average coercive field is about 96 MV m^{-1}, which is larger than, but still comparable to that of the copolymer bulk counterpart (50 MV m^{-1}). One possible reason could be that the interfacial interaction between the copolymer and FeGa changes the ferroelectric switching behavior when the shell thickness is scaled down to the

nanometer range.[17] Another important fact is that, in PFM measurements the switching bias field is applied via a sharp tip, and thus the field is inhomogeneous as opposed to conventional ferroelectric tests. Nevertheless, since the tip is fixed at the same point, the values obtained with or without the magnetic field are still comparable. Under magnetic field, the coercive voltages become -4.56 V and 0.28 V, respectively, corresponding to an average coercive field of 69 MV m^{-1}. The smaller coercive field obtained under magnetic field indicates that the strain generated in the magnetostrictive FeGa core is effectively transferred onto the shell, facilitating the polarization reversal process in P(VDF-TrFE). This is direct evidence of strain mediated magnetoelectric effect in the composite nanowire.

We note that the positive coercive voltage change (1.28 V) is larger than the negative coercive voltage change (0.62 V). The asymmetric change means that there is an offset of the center of the piezoresponse loop under magnetic field, which is supposed to be caused by an electric field generated by the ME effect.[18] As is known, the ME coupling coefficient is defined as

$$\alpha_E = \Delta E / \Delta H \quad (1)$$

where ΔH is the increment in the external magnetic field and ΔE is the increment in the electric field caused by the external magnetic field.[18] In our case, the electric field change ΔE, i.e. the offset of the center of the loop upon application of magnetic field, is estimated to be (1.28 V-0.62 V)/2/35 nm= 9.4 MV m^{-1}. Then, the local ME coefficient can be estimated as 9.4×10^4 mV cm^{-1} Oe^{-1}. This is the first report of a direct magnetoelectric effect in the composite of FeGa/PVDF ferroelectric polymer. This value is in the same order as those reported for some other one dimensional core-shell nanostructures (e.g., $CoFe_2O_4$@$PbZr0_{.52}Ti_{0.48}O_3$, $CoFe_2O_4$@$BaTiO_3$, $CoFe_2O_4$@$BiFeO_3$) evaluated by similar methods.[13a, 19] However, it should be noted that such

local measurements cannot be compared directly to the macroscopic ME coefficient, although some recent theoretical analysis indicates that composite multiferroic nanowires could potentially exhibit a ME response orders of magnitude higher than that of thin films with similar compositions.[20]

For effective site-specific drug delivery, especially for chemotherapeutics with severe side effects, an ideal administration method employs non-cytotoxic nano-carriers to carry drugs to the lesion, and then releases the drugs on demand by an externally controlled triggering mechanism. Here, we demonstrate this concept using magnetoelectric nanowires under the application of various forms of magnetic fields. First, to realize targeted therapeutics, precise control of locomotion and maneuvering of the nanowire robot is essential. Nanowire propulsion falls under the low Reynolds number Stoke's flow regime, where viscous forces dominate over inertial forces, rendering conventional macroscopic locomotion schemes inappropriate.[21] Here, we demonstrate two strategies that can actuate a single nanowire at low Reynolds number using the torque generated on the magnetic nanowire by low amplitude (< 10mT) rotating magnetic fields. The first motion strategy is based on a near surface-effect which we call a tumbling or surface-walking motion,[22] where the nanowire is propelled forward and steered i.e., it executes rotation along with translation on a surface. The second strategy endows the nanowire with the ability to swim in three dimensions (3D). This is the first report showing that a rigid nanowire can be manipulated to swim in 3D.

Manipulation experiments were conducted in a specially designed set-up with three orthogonal electromagnetic coil pairs. [4a] Surface-walking tests were performed near a flat Si surface in deionized water, shown schematically in **Figure 3a**. It is known that the magnetic nanowire can follow the rotating magnetic field with their long axis. To rotate the nanowire on the

surface, one needs to set the rotating plane perpendicular to the surface. In this configuration, the hydrodynamic interaction of the nanowire with the surface is stronger on one end than on the other, leading to a velocity difference between the two ends of the nanowire. The asymmetric boundary condition breaks the time reversibility of the motion, resulting in a "surface-walker" motion. The parameter α in Figure 3a controls the orientation of "surface-walker" motion. In order to steer the tumbling motion, only the input parameter α has to be changed. Figure 3b shows the optical top-view of the precise steering of the nanowire along a predefined trajectory (also see Supplementary Video S1). The dependence of the average translational velocity of the nanowire on the rotation frequency was characterized, as shown in Figure 3c. The results shows a linear relationship between the input field frequency and the velocity when the nanowire rotates in sync with the input field. Using the same technique, the nanowire can climb up and down a vertical wall (Figure 3d and Supplementary Video S2). A micro channel with width of 20 μm and depth of 6 μm is fabricated through photolithography. The nanowire is first propelled toward the wall of the microchannel, where it overcomes its weight and tumbles upward along the vertical wall of the channel. After climbing out of the channel, the nanowire "walks" around the surface and then down into the channel again. The climbing test demonstrates the feasibility of propelling the nanowire near a complex surface.

Next we present a novel 3D propulsion mode for the nanowires, actuated by a conical rotating magnetic field. In sync with the conical field, the magnetic nanowire rotates on a conical surface around the axis of rotation. The upper and lower part of the conical surface is asymmetric, and this asymmetry results in a translational force on the nanowire (Figure 3e). Figure 3f and Supplementary Video S3 show that a rigid nanowire can be driven by this method until it "lifts off" from the surface. At t=2 s, the nanowire speed up to rotate on the surface. After applying a conical

field, the nanowire gradually swims up until it goes out of focus (t=7 s). To change the swimming direction, we can control the direction of the axis of rotation by adjusting the pitch angle θ (Figure 3g). We demonstrate the precise three-dimensional swimming of the nanowire along a predefined trajectory (Figure 3h and Supplementary Video S4). The nanowire swims over a micropillar (height of 6 μm), which is clear evidence of motion in 3D. However, it is worth noting that in biological fluids such as serum, the viscosity, temperature and components of the fluid may dramatically influence the swimming behavior of the nanorobots.[23]

Besides targeted motion, on-site controlled drug release is another important factor for effective therapeutics. First, we verified the biocompatibility of the nanowires to make sure that they can be used as drug delivery vehicles. We observed that up to a concentration of 100 ppm cell viability is not affected (Figure S4). To facilitate drug loading, the nanowires were pretreated with polydopamine (PDA), which introduced a large amount of amine and hydroxyl groups on their surface. [24] Paclitaxel, a drug widely used to treat ovarian, breast, lung, pancreatic and other cancers, is adsorbed onto the surface of the core-shell nanorobots. The adsorption occurs most probably through the interaction (e.g. hydrogen bond, Van der Waals, etc.) between amine, hydroxyl and carbonyl groups in paclitaxel and polydopamine. When the drug delivery system is exposed to an alternating magnetic field, the transient changes of polarization state brought by the magnetoelectric effect breaks the interaction between the drug molecules and polydopamine, and thereby releases the drug (**Figure 4**a). The results confirm our hypothesis. Figure 4b shows that the viability of the cells cultured with the drug-loaded nanowires under an AC magnetic field (Figure 4b (i)) is decreased by ~40% compared with that of the control sample (Figure 4b (ii)). Multiple control experiments were carried out to confirm that the cancer cells were not killed by magnetic hyperthermia (Figure 4b (iii)) and diffusion of the drug molecule (Figure 4b (iv)).

Therefore, we can conclude that the drug release is mostly due to the magnetoelectric effect of the nanowires. Note that the application of a DC magnetic field did not cause any significant cell death as compared to the control sample (Figure 4b (v)). The phenomena may be due to the fact that the transient changes in polarization states on the surface are immediately compensated by adsorbed charges, and no further changes can be induced to release the drugs due to the invariant magnetic field. The unique feature (i.e. drug molecules released largely by AC fields but not much by DC fields) indicates that side effects to the healthy tissue can be minimized during the drug transportation process, where the nanowire is maneuvered to the targeted lesion using a rotating magnetic field with invariant magnitude.

In summary, we have fabricated FeGa@P(VDF-TrFE) core-shell magnetoelectric nanowires and demonstrated that they can be actuated and triggered using different magnetic fields for targeted drug delivery. Ferroelectric P(VDF-TrFE) nanotubes are first obtained by melt-wetting of AAO templates. Subsequent electrodeposition of FeGa allows conformal growth of the magnetostrictive core. The fabrication strategy allows facile tuning of geometric parameters (i.e. length and diameter) of the nanowire, and more importantly, superior interfacial coupling between piezoelectric and magnetostrictive phases. Structural characterization (IR, XRD, and EDX) confirms that P(VDF-TrFE) and FeGa is in the proper piezoelectric and magnetostrictive phase, respectively. Ferroelectricity in the nanotube is further confirmed using piezoresponse force microscopy. Distinct domain switching characteristics in the nanowire with or without external magnetic field are observed, indicating prominent magnetoelectric coupling. The nanowires are able to load the anti-cancer drug paclitaxel after surface functionalization using polydopamine, and release the drug upon the application of alternating magnetic fields due to the magnetoelectric effect. Therefore, cancer cells are killed by the released drug. We demonstrate precise magnetic

maneuvering capabilities on a patterned surface and 3D swimming using low amplitude rotating magnetic fields. The precise control strategy provides the nanowires with superior targeting ability. Distinct magnetic stimuli resulting from the same energy source – alternating magnetic fields for drug release, and rotating magnetic fields for nanowire steering – enables these devices to carry and deliver drugs effectively to the targeted site while minimizing side effects of drugs administered systemically. The proposed nanomachines represent a further step in the development of miniaturized magnetoelectric platforms for biomedical applications.

Acknowledgements

X. C. and S. P. conceived the idea. X. C. fabricated the nanowires. X. C., N. S., Q. L. did the PFM measurements. M. H., L. D. T. did the drug delivery experiments. N. S. and E. S. built the magnetic field generator and cell incubation system. T. H. did the magnetic manipulation of nanowires. B. Ö. took the TEM images and the SAED patterns. B. Ö. and F. M. deposited carbon using FIB. All of the authors contributed to writing the manuscript. This work has been financed by the European Research Council Starting Grant "Magnetoelectric Chemonanorobotics for Chemical and Biomedical Applications (ELECTROCHEMBOTS) under the grant no. 336456. The authors would like to acknowledge Joël Vermeulen and Viktor Jooss for their help in designing the magnetic field generator, Lydia Zehnder from Institute für Geochemie und Petrologie of ETH for her kind support on XRD measurements, Dr. Zhongshu Li at Department of Chemistry and Applied Biosciences for his help on IR measurements, the Scientific Center for Optical and Electron Microscopy (ScopeM) of ETH and the FIRST laboratory for their technical support.

Received: ((will be filled in by the editorial staff))

Revised: ((will be filled in by the editorial staff))

Published online: ((will be filled in by the editorial staff))

References

[1] a) S. Kim, F. Qiu, S. Kim, A. Ghanbari, C. Moon, L. Zhang, B. J. Nelson, H. Choi, *Adv. Mater.* **2013**, *25*, 5863; b) S. Fusco, M. S. Sakar, S. Kennedy, C. Peters, R. Bottani, F. Starsich, A. Mao, G. A. Sotiriou, S. Pane, S. E. Pratsinis, D. Mooney, B. J. Nelson, *Adv. Mater.* **2014**, *26*, 952; c) T. Y. Huang, M. S. Sakar, A. Mao, A. J. Petruska, F. Qiu, X. B. Chen, S. Kennedy, D. Mooney, B. J. Nelson, *Adv. Mater.* **2015**, *27*, 6644; d) C. Peters, M. Hoop, S. Pane, B. J. Nelson, C. Hierold, *Adv. Mater.* **2016**, *28*, 533; e) B. J. Nelson, I. K. Kaliakatsos, J. J. Abbott, *Annu. Rev. Biomed. Eng.* **2010**, *12*, 55.

[2] a) H. Wang, M. Pumera, *Chem. Rev.* **2015**, *115*, 8704; b) S. Sanchez, L. Soler, J. Katuri, *Angew. Chem. Int. Ed.* **2015**, *54*, 1414; c) W. Gao, J. Wang, *Nanoscale* **2014**, *6*, 10486; d) M. Medina-Sánchez, L. Schwarz, A. K. Meyer, F. Hebenstreit, O. G. Schmidt, *Nano Lett.* **2016**, *16*, 555.

[3] a) F. Qiu, R. Mhanna, L. Zhang, Y. Ding, S. Fujita, B. J. Nelson, *Sensors and Actuators B: Chemical* **2014**, *196*, 676; b) F. Qiu, S. Fujita, R. Mhanna, L. Zhang, B. R. Simona, B. J. Nelson, *Adv. Funct. Mater.* **2015**, *25*, 1666; c) M. Hoop, F. Mushtaq, C. Hurter, X. Z. Chen, B. J. Nelson, S. Pane, *Nanoscale* **2016**, *8*, 12723.

[4] a) L. Zhang, J. J. Abbott, L. Dong, B. E. Kratochvil, D. Bell, B. J. Nelson, *Appl. Phys. Lett.* **2009**, *94*, 064107; b) W. Wang, T.-Y. Chiang, D. Velegol, T. E. Mallouk, *J. Am. Chem. Soc.* **2013**, *135*, 10557; c) J. Parmar, X. Ma, J. Katuri, J. Simmchen, M. M. Stanton, C. Trichet-Paredes, L. Soler, S. Sanchez, *Sci. Tech. Adv. Mater.* **2015**, *16*; d) D. Ahmed, C. Y. Chan, S. C. Lin, H. S. Muddana, N. Nama, S. J. Benkovic, T. J. Huang, *Lab Chip* **2013**, *13*, 328; e) D. Ahmed, M. Lu, A. Nourhani, P. E. Lammert, Z. Stratton, H. S. Muddana, V. H. Crespi, T. J. Huang, *Sci. Rep.* **2015**, *5*, 9744.

[5] M. P. Kummer, J. J. Abbott, B. E. Kratochvil, R. Borer, A. Sengul, B. J. Nelson, *IEEE Trans. Robotic.* **2010**, *26*, 1006.

[6] a) M. Nair, R. Guduru, P. Liang, J. Hong, V. Sagar, S. Khizroev, *Nat. Commun.* **2013**, *4*, 1707; b) R. Guduru, S. Khizroev, *Part. Part. Syst. Charact.* **2014**, *31*, 605; c) K. Yue, R. Guduru, J. Hong, P. Liang, M. Nair, S. Khizroev, *PloS one* **2012**, *7*, e44040; d) R. Guduru, P. Liang, C. Runowicz, M. Nair, V. Atluri, S. Khizroev, *Sci. Rep.* **2013**, *3*, 2953; e) X. Z. Chen, N. Shamsudhin, M. Hoop, R. Pieters, E. Siringil, M. S. Sakar, B. J. Nelson, S. Pané, *Mater. Horiz.* **2016**, *3*, 113.

[7] a) M. Steinhart, J. H. Wendorff, A. Greiner, R. B. Wehrspohn, K. Nielsch, J. Schilling, J. Choi, U. Gosele, *Science* **2002**, *296*, 1997; b) C.-C. Wang, Q.-D. Shen, S.-C. Tang, Q. Wu, H.-M. Bao, C.-Z. Yang, X.-Q. Jiang, *Macromol. Rapid. Commun.* **2008**, *29*, 724; c) J. Martin, J. Maiz, J. Sacristan, C. Mijangos, *Polymer* **2012**, *53*, 1149; d) K. Choi, S. C. Lee, Y. Liang, K. J. Kim, H. S. Lee, *Macromolecules* **2013**, *46*, 3067.

[8] a) A. E. Clark, J. B. Restorff, M. Wun-Fogle, T. A. Lograsso, D. L. Schlagel, *IEEE Trans. Magn.* **2000**, *36*, 3238; b) A. E. Clark, M. Wun-Fogle, J. B. Restorff, T. A. Lograsso, J. R. Cullen, *IEEE Trans. Magn.* **2001**, *37*, 2678.

[9] a) X. Z. Chen, Q. Li, X. Chen, X. Guo, H. X. Ge, Y. Liu, Q. D. Shen, *Adv. Funct. Mater.* **2013**, *23*, 3124; b) X. Z. Chen, X. Chen, X. Guo, Y. S. Cui, Q. D. Shen, H. X. Ge, *Nanoscale* **2014**, *6*, 13945; c) M. C. Garcia-Gutierrez, A. Linares, I. Martin-Fabiani, J. J. Hernandez, M. Soccio, D. R. Rueda, T. A. Ezquerra, M. Reynolds, *Nanoscale* **2013**, *5*, 6006; d) J. L. Lutkenhaus, K. McEnnis, A. Serghei, T. P. Russell, *Macromolecules* **2010**, *43*, 3844.

[10] a) R. Ramesh, N. A. Spaldin, *Nat. Mater.* **2007**, *6*, 21; b) Y. H. Chu, L. W. Martin, M. B. Holcomb, M. Gajek, S. J. Han, Q. He, N. Balke, C. H. Yang, D. Lee, W. Hu, Q. Zhan, P. L. Yang, A. Fraile-Rodriguez, A. Scholl, S. X. Wang, R. Ramesh, *Nat. Mater.* **2008**, *7*, 478; c) J. Ma, J. M. Hu, Z. Li, C. W. Nan, *Adv. Mater.* **2011**, *23*, 1062; d) J. Jin, S. G. Lu, C. Chanthad, Q. Zhang, M. A. Haque, Q. Wang, *Adv. Mater.* **2011**, 3853; e) S. G. Lu, J. Z. Jin, X. Zhou, Z. Fang, Q. Wang, Q. M. Zhang, *J. Appl. Phys.* **2011**, *110*, 104103.

[11] a) H. S. Nalwa, *Ferroelectric polymers: Chemistry, physics, and applications*, Marcel Dekker, New York **1995**; b) H. M. Bao, J. F. Song, J. Zhang, Q. D. Shen, C. Z. Yang, Q. M. Zhang, *Macromolecules* **2007**, *40*, 2371.

[12] a) S. M. Reddy, J. J. Park, S. M. Na, M. M. Maqableh, A. B. Flatau, B. J. H. Stadler, *Adv. Funct. Mater.* **2011**, *21*, 4677; b) D. Iselt, A. Funk, L. Schultz, H. Schlorb, *ECS Electrochem. Lett.* **2013**, *2*, D13.

[13] a) S. H. Xie, F. Y. Ma, Y. M. Liu, J. Y. Li, *Nanoscale* **2011**, *3*, 3152; b) G. Caruntu, A. Yourdkhani, M. Vopsaroiu, G. Srinivasan, *Nanoscale* **2012**, *4*, 3218.

[14] a) Y. M. Liu, D. N. Weiss, J. Y. Li, *ACS Nano* **2010**, *4*, 83; b) S. Jesse, A. P. Baddorf, S. V. Kalinin, *Appl. Phys. Lett.* **2006**, *88*, 062908.

[15] S. Kalinin, D. Bonnell, *Phys. Rev. B* **2002**, *65*.

[16] X. Gao, B. J. Rodriguez, L. Liu, B. Birajdar, D. Pantel, M. Ziese, M. Alexe, D. Hesse, *ACS Nano* **2010**, *4*, 1099.

[17] a) R. C. G. Naber, P. W. M. Blom, A. W. Marsman, D. M. de Leeuw, *Appl. Phys. Lett.* **2004**, *85*, 2032; b) F. Xia, H. S. Xu, F. Fang, B. Razavi, Z. Y. Cheng, Y. Lu, B. M. Xu, Q. M. Zhang, *Appl. Phys. Lett.* **2001**, *78*, 1122; c) H. S. Xu, J. H. Zhong, X. B. Liu, J. H. Chen, D. Shen, *Appl. Phys. Lett.* **2007**, *90*, 092903.

[18] H. Miao, X. Zhou, S. Dong, H. Luo, F. Li, *Nanoscale* **2014**, *6*, 8515.

[19] a) B. Fu, R. Lu, K. Gao, Y. Yang, Y. Wang, *EPL-Europhys. Lett.* **2015**, *112*, 27002; b) Q. Zhu, Y. Xie, J. Zhang, Y. Liu, Q. Zhan, H. Miao, S. Xie, *J. Mater. Res.* **2014**, *29*, 657.

[20] C. L. Zhang, W. Q. Chen, S. H. Xie, J. S. Yang, J. Y. Li, *Appl. Phys. Lett.* **2009**, *94*, 102907.

[21] a) E. M. Purcell, *Am. J. Phys.* **1977**, *45*, 3; b) J. J. Abbott, K. E. Peyer, M. C. Lagomarsino, L. Zhang, L. Dong, I. K. Kaliakatsos, B. J. Nelson, *Int. J. Robot. Res.* **2009**, *28*, 1434; c) G. A. Ozin, I. Manners, S. Fournier-Bidoz, A. Arsenault, *Adv. Mater.* **2005**, *17*, 3011.

[22] a) T. Petit, L. Zhang, K. E. Peyer, B. E. Kratochvil, B. J. Nelson, *Nano Lett.* **2012**, *12*, 156; b) L. Zhang, T. Petit, Y. Lu, B. E. Kratochvil, K. E. Peyer, R. Pei, J. Lou, B. J. Nelson, *ACS Nano* **2010**, *4*, 6228.

[23] L. Soler, C. Martinez-Cisneros, A. Swiersy, S. Sanchez, O. G. Schmidt, *Lab Chip* **2013**, *13*, 4299.

[24] a) H. Lee, S. M. Dellatore, W. M. Miller, P. B. Messersmith, *Science* **2007**, *318*, 426; b) G.-d. Kang, Y.-m. Cao, *J. Membrane Sci.* **2014**, *463*, 145; c) L. Shao, Z. X. Wang, Y. L. Zhang, Z. X. Jiang, Y. Y. Liu, *J. Membrane Sci.* **2014**, *461*, 10.

Figure 1. (a) Fabrication scheme of FeGa@P(VDF-TrFE) core-shell nanowires. (b) AFM image of two nanowires with FeGa grown out of P(VDF-TrFE) nanotubes. The arrow indicates the growth direction of FeGa. (c) TEM image of a core-shell nanowire. The inset shows the cross-sectional grayscale profile along the dashed line. (d) FTIR spectrum of P(VDF-TrFE) nanotubes. (e) XRD pattern showing crystalline structure of FeGa@P(VDF-TrFE) core-shell nanowires. The inset shows the SAED pattern of a single nanowire.

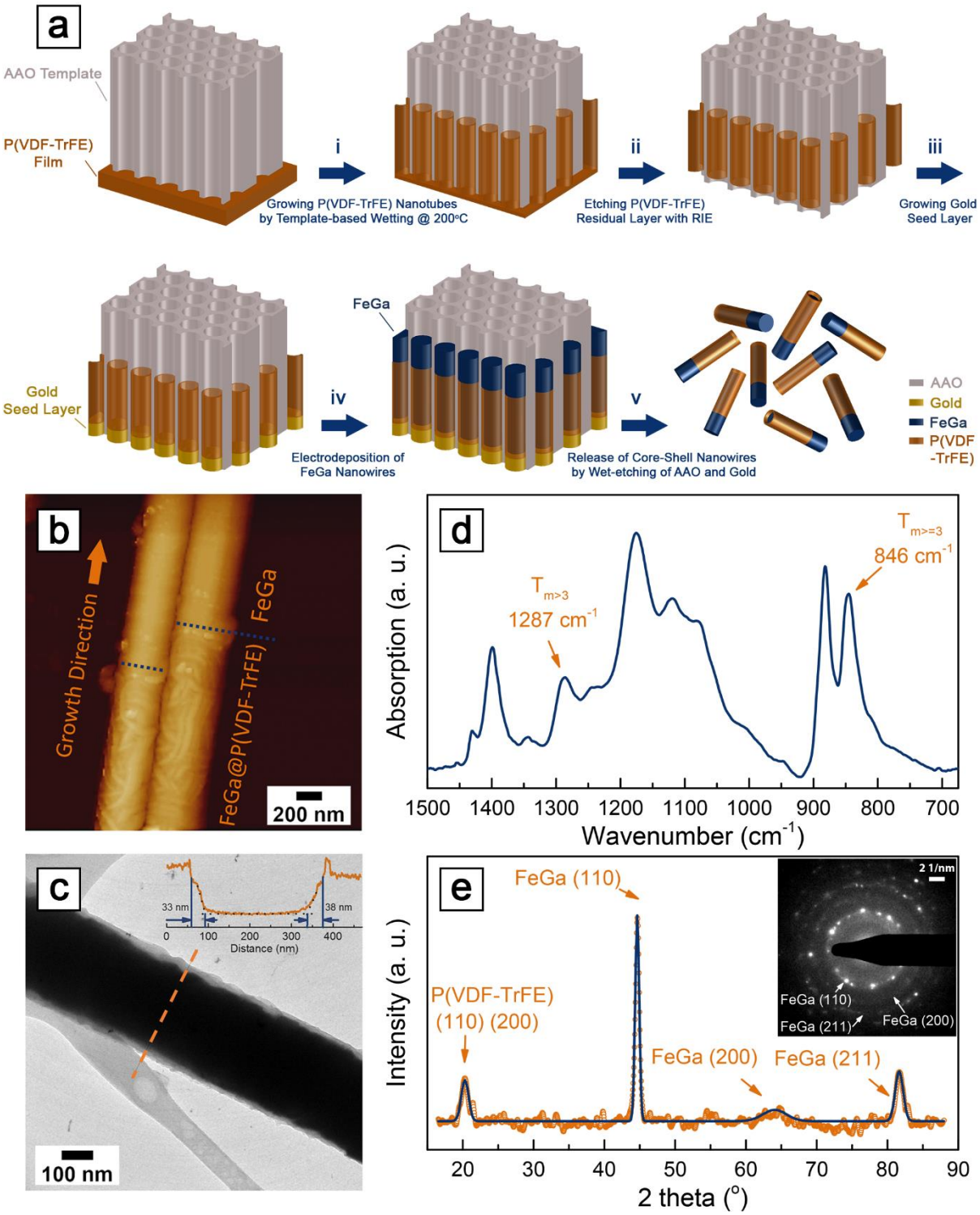

Figure 2. PFM phase (a, c) and amplitude (b, d) images of FeGa@P(VDF-TrFE) core-shell nanowires without (first row) and with (second row) magnetic field. All the scale bars in the images are 200 nm. Piezoresponse amplitude (e) and phase (f) loops obtained from the FeGa@P(VDF-TrFE) core-shell nanowires without (solid blue triangle) and with (hollow orange circle) magnetic field.

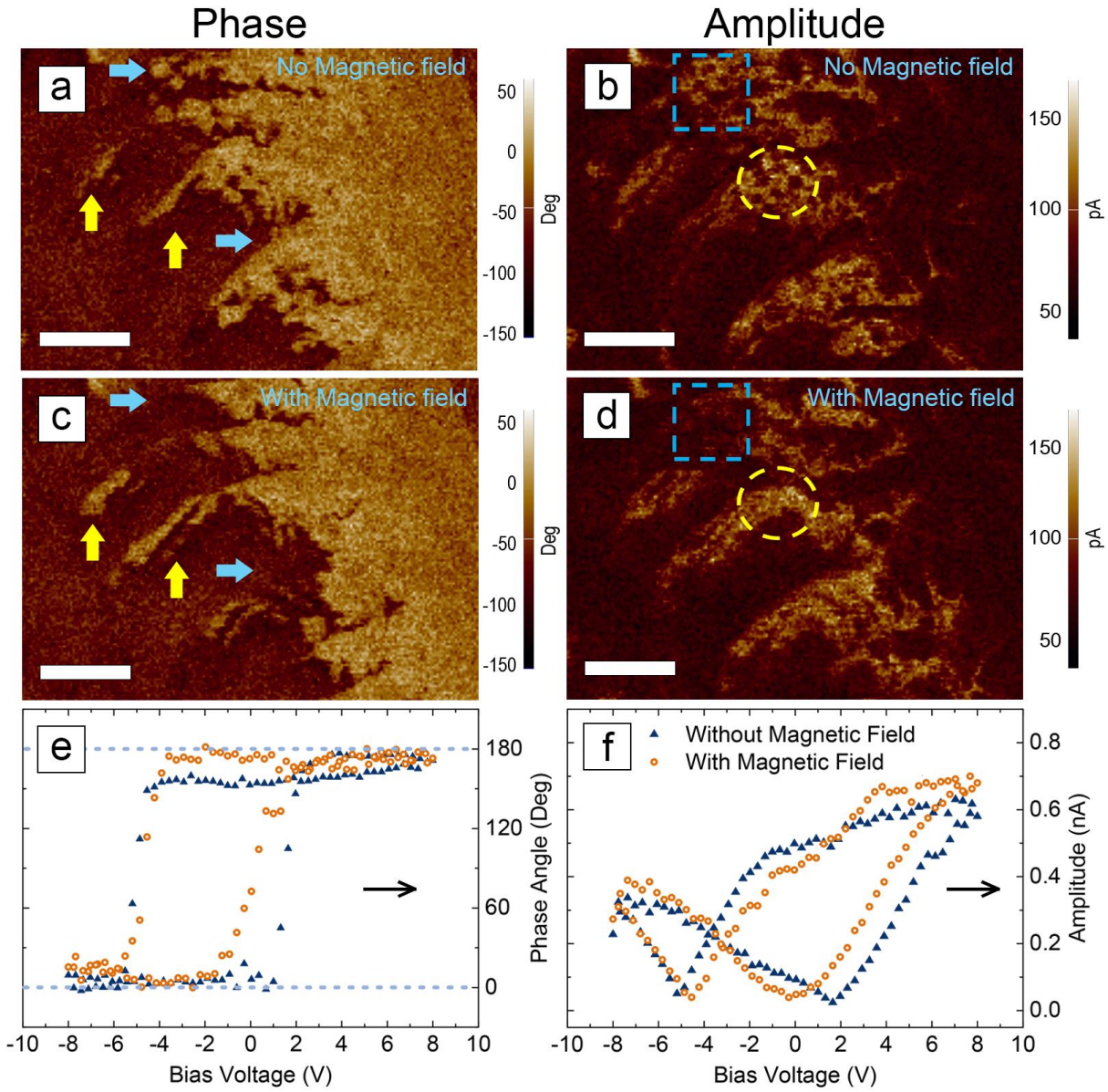

Figure 3. (a) Schematic illustration of the nanowire rotating vertically with respect to the x-y plane. (b) The nanowire is manipulated to follow the shape of a heart. (c) Average translational velocity with respect to the magnetic field frequency. (d) Demonstration of nanowire climbing up a step of 6 μm high. (e) Schematic illustration of the motion of a core-shell nanowire in a conical rotating magnetic field. (f) A core-shell nanowire moving away from the surface under the manipulation of a conical rotating magnetic field. (g) Schematic illustration of steering the nanowire by changing the translational motion direction. (h) The nanowire is steered to swim following a U-shaped trajectory. Scale bars in figure 3(f) and (h) represent 5 μm.

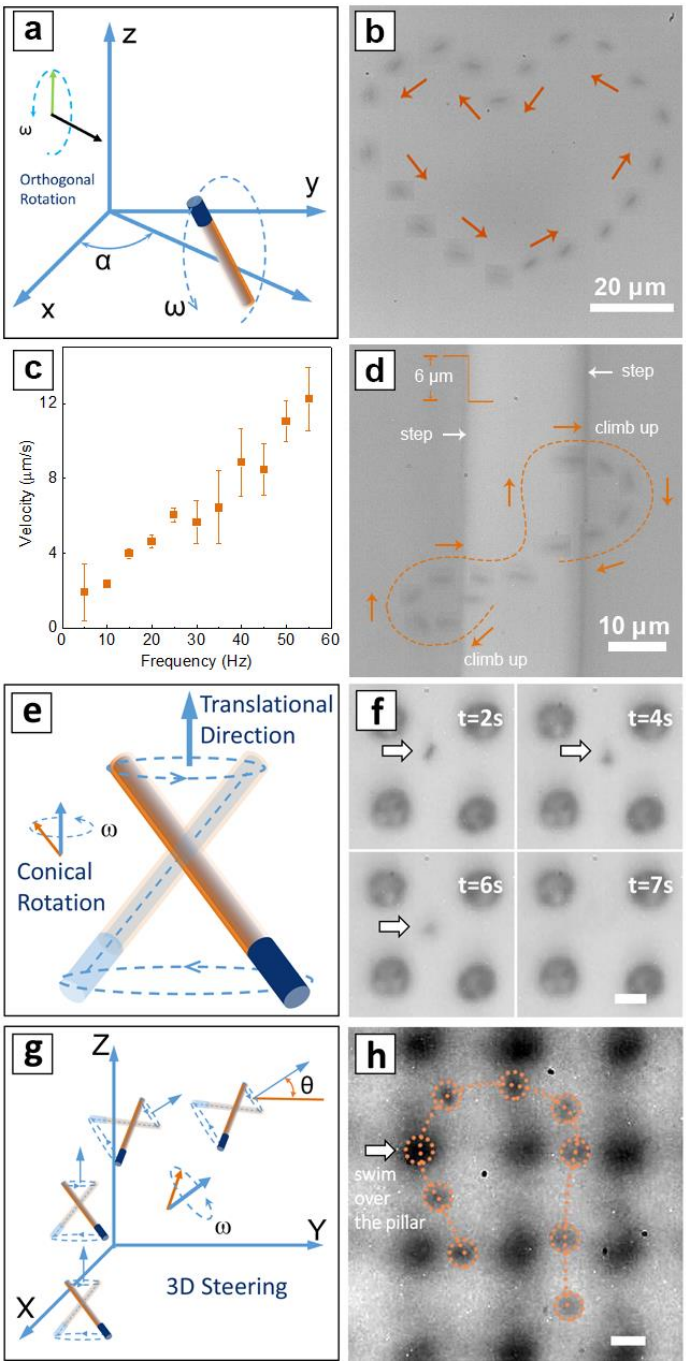

Figure 4. (a) Scheme showing on-demand drug delivery experiment. The anti-cancer drug is loaded onto a PDA treated FeGa@P(VDF-TrFE) core-shell nanowire and then released by applying an alternating magnetic field. PDA: polydopamine. PTX: Paclitaxel. (b) The efficacy of AC field triggered on demand drug delivery experiment in comparison to several control experiments.

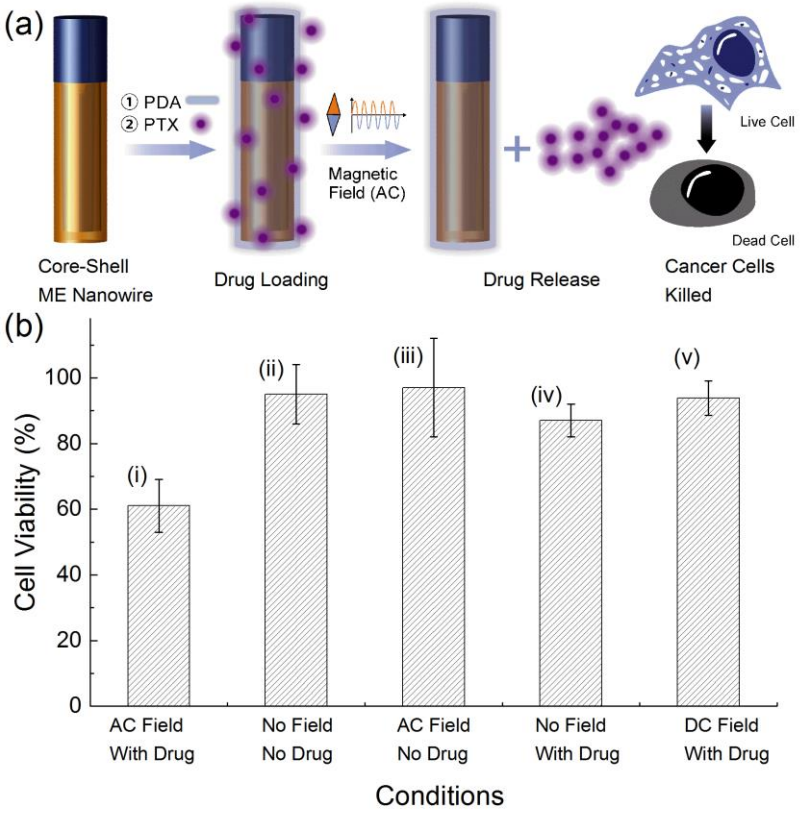

Table of contents entry

A FeGa@P(VDF-TrFE) wire-shaped magnetoelectric nanorobot is designed and fabricated to demonstrate a proof-of-concept integrated device, which features wireless locomotion and on-site triggered therapeutics with a single external power source (i.e. a magnetic field). The device can be precisely steered towards a targeted location wirelessly by rotating magnetic fields and perform on-demand magnetoelectrically-assisted drug release to kill cancer cells.

Keywords: Nanorobotics, Magnetoelectric, P(VDF-TrFE), FeGa, Drug delivery

Xiang-Zhong Chen, Marcus Hoop, Naveen Shamsudhin, Tianyun Huang, Berna Özkale, Qian Li, Erdem Siringil, Fajer Mushtaq, Luca Di Tizio, Bradley J. Nelson, and Salvador Pané*

Title: Hybrid Magnetoelectric Nanowires for Nanorobotic Application: Fabrication, Magnetoelectric Coupling and Magnetically-assisted *in vitro* Targeted Drug Delivery